



Research Article

Green synthesis and anticorrosion effect of *Allium cepa* peels extract-silver nanoparticles composite in simulated oilfield pickling solution

Ekemini Ituen^{1,2,3} · Ambrish Singh^{1,2} · Lin Yuanhua^{1,2} · Onyewuchi Akaranta⁴

Received: 16 April 2020 / Accepted: 19 May 2021

Published online: 31 May 2021

© The Author(s) 2021 **OPEN**

Abstract

An alternative green approach through which nanoscience/nanotechnology could be applied in the industry is being demonstrated in this study. Ethanol extracts of *Allium cepa* peels (Et-ACPE) is used to mediate the synthesis of silver nanoparticles (Et-AgNPs) at room temperature. Stable crystalline, monodisperse and non-agglomerated spherical NPs with zeta potential of -46.2 ± 0.1 mV and plasmon absorption at 435 nm are obtained. Silver atoms are predominantly oriented towards the Ag (111) plane in a face centered cubic structure with $a = b = c = 4.0968$ Å having $\alpha = \beta = \gamma = 90^\circ$. The surfaces of the NPs becomes rich in electron cloud due to O atoms supplied by capped phyto-compounds of Et-ACPE. This enhances adsorption potential and more efficient inhibition (up to 90% at 30 °C) of X80 steel corrosion in 1 M HCl solution than using the crude extract. Investigation of corrosion products and morphologies of the steel surface by FTIR, SEM/EDS and AFM techniques reveals efficient surface protection through adsorption of Et-AgNPs facilitated mainly by O and $-C=C-$ sites. Findings prove that the Et-AgNPs is a more efficient and thermally stable alternative ecofriendly anticorrosion additive for industrial cleaning and pickling operations than the crude extract.

Keywords Anticorrosion · Nanoparticles · Oilfield chemical · XRD · TEM · SEM/EDS

1 Introduction

Hydrochloric acid (HCl) is an important inorganic acid that has been extensively used as industrial cleaning solution. Also called muriatic acid, it is used for cleaning surfaces of various metals and alloys, including steel, especially to remove scales, rust and mineral deposits. In general, HCl used is for chemical cleaning/pickling of steel, reduction of ores and processing, industrial preparation of chlorine and

chlorides, acid treatment of oil and gas wells and in food processing [1]. However, HCl is known for its high corrosivity, and depending on temperature under which operation is carried out and the concentration of the acid used, it can rather be aggressive to and corrode the surfaces meant to be cleaned. To ameliorate the corrosive damage, materials selection has been the practice by many industries, but there is limited choice for potential corrosion resistant materials in HCl. This is because on continuous contact of

Supplementary information The online version contains supplementary material available at <https://doi.org/10.1007/s42452-021-04670-w>.

✉ Ekemini Ituen, ebituen@gmail.com; ✉ Lin Yuanhua, yhlin28@163.com | ¹State Key Laboratory of Oil and Gas Reservoir Geology and Exploitation, Southwest Petroleum University, Chengdu 610500, Sichuan, China. ²School of Materials Science and Engineering, Southwest Petroleum University, Chengdu 610500, Sichuan, China. ³Emerging Materials and Energy Research Group, Department of Chemistry, University of Uyo, Uyo, Nigeria. ⁴African Center of Excellence in Oilfield Chemicals Research, Institute of Petroleum Studies, University of Port Harcourt, Port Harcourt, Nigeria.



SN Applied Sciences

(2021) 3:679

| <https://doi.org/10.1007/s42452-021-04670-w>

SN Applied Sciences
A **SPRINGER NATURE** journal

the material with HCl, localized and/or general corrosion will still occur which may eventually result in failure of the material. Therefore, corrosion inhibitors need to be formulated into the acid to reduce HCl corrosive attack [2].

Added in very small quantities, corrosion inhibitors (CIs) act by adsorbing on the substrate surface and forming a surface protective thin film [3]. To select CI for a given operation, cost effectiveness, low toxicity and environmental friendliness, efficiency at small concentrations, stability to varying operational temperatures and shelf life are some crucial factors to be considered [4, 5]. Bearing these factors in mind, green CIs sourced from plant extracts often afford combined advantage over many organic CIs. Nevertheless, plant extracts are not resistant to degradation by heat or biochemical agents, hence their application is limited to low temperature operations. Also, if stored for long time, the efficiency of plant extracts often decline [5].

In recent researches, attention has been paid to how plant extracts may be modified to improve stability at high temperatures and resistance to bio-degradation. Extracts have been mixed with some additives such as potassium iodide [6–8], acetylacetonate [9], cerium nitrate [10], zinc oxide and zinc salt [11–13], sulphate ions [14] and praseodymium nitrate [15]. These additives enhanced the performance of plant extracts by synergistic effects [5]. Reaction between some active chemical compounds in plant extracts with metal salts may result in formation of metal ions complexes and/or nanoparticles (NPs) at appropriate biomass (extract) concentration, temperature and pH. In the previously listed reports [6–14] where metal salts were used to synergistically intensify the efficiency of the CIs, nothing was done to confirm if the obtained product was in nano scale despite that materials are more reactive at nanoscale.

Synthesis of plant extracts nanoparticles often involve a single step bio-reduction reaction that occurs within short time even at room temperature [16]. Though NPs can be prepared by various routes, bio-synthetic pathway affords the advantage of obtaining the inexpensive, non-toxic and eco-environmental NPs in large quantities. Owing to their vast antimicrobial activities, bio-fabricated NPs have been applied in agriculture, medicine and pharmaceuticals [17]. In comparison to other metal ions, silver nanoparticles (AgNPs) are the most extensively reported. AgNPs have been established to exhibit antiprotozoal, antibacterial, antifungal and anticancer activities [17–21]. This has been attributed to slightly toxic nature of silver ions to the target. Silver ions reduce their growth/multiplication by tampering with their cell membrane [16, 18]. Although many plant extracts have been demonstrated to efficiently inhibit corrosion, evaluating plant extract mediated NPs as CIs has received only little attention. In this study, we explore future research horizon in corrosion protection using plant extract mediated

nanoparticles (PEMN) especially considering that there is a wide variety of plant materials which could be investigated.

From available literature, PEMN with anticorrosion activity was recently reports by Essien and co-workers [19] and Idrees and co-workers [20]. They used olive leaves [19] and *Sida acuta* [20] extracts as feedstock for fabrication of titanium and silver nanoparticles composites, respectively. For the *Sida acuta* mediated AgNPs potentiodynamic polarization method only was used to monitor corrosion progress in 0.5 M H₂SO₄ for 30 min while the biocide activity was more emphasized. Titanium NPs from olive leaves extract were to be used as adsorbents for scavenging heavy metal ions from waste water. In the process of studying the material, the authors also evaluated its anti-corrosion effect. Since the obtained efficiency in HCl for steel was encouraging, it motivated us to evaluate extracts of some agro-wastes to develop more efficient biogenic NPs as alternative CIs for oilfield pickling. Agro-wastes are inexpensive and can be sustainably sourced locally as long as food is continually being consumed. Again, utilization of agro-wastes for corrosion protection eliminates competition of feedstock with food, could reduce environmental pollution while creating wealth from wastes.

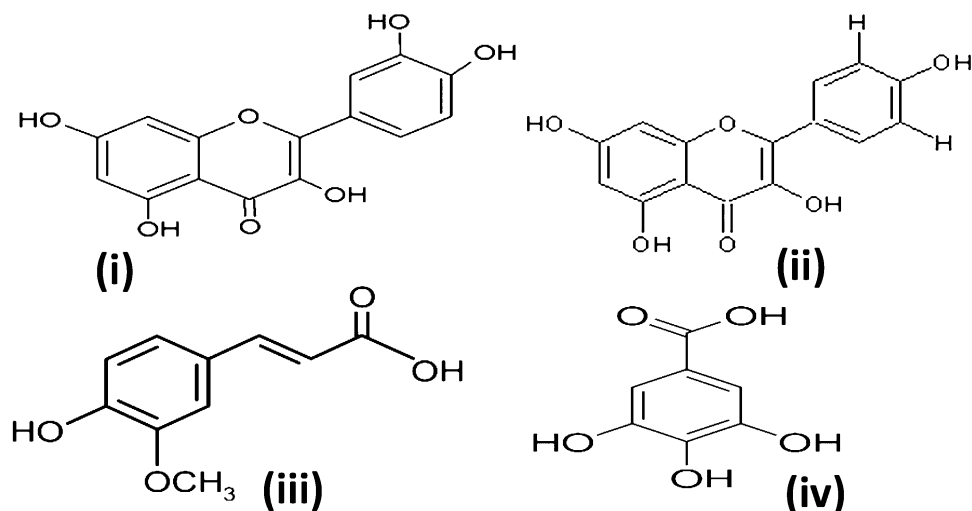
In our previous (recent) reports, we have demonstrated that some PEMN using Cu, Ni and Ag ions mediated exhibit better inhibition potential than previously reported NPs [18, 21, 22]. By using silver ions as capping agent and *Allium cepa* peels extract (ACPE) as catalyst, the present study also aims to achieve improved efficiency. *Allium cepa* (red onion) peels is can be domestically obtained without the need to buy. ACPE has been to contain more compounds than the inner shells [23, 24] and on observing the molecular structures of some of these compounds (Fig. 1) potential adsorption sites similar to those in reported organic corrosion inhibitors can be seen [25]. The availability of potential adsorption sites such as O–H, C–O–C, –COO– shown in Fig. 1 motivated the choice of ACPE as a feedstock for synthesis of the nanoscale corrosion inhibitor. Already, it is established that peels extract of red onions can inhibit steel corrosion in some aggressive solutions [26–28]. The present study therefore builds on these foundation reports and in addition provides/documents further insights on the optical/crystalline properties, adsorption behaviour and corrosion inhibition effects of PEMN.

2 Experimental

2.1 Preparation of *A. cepa* peels extract (ACPE)

Allium cepa peels (ACP) were obtained from sellers of onions at a nearby market to our university. The peels

Fig. 1 Some major chemical compounds in *Allium cepa* extracts, namely (i) quercetin (ii) kaempferol (iii) ferulic acid and (iv) gallic acid



were washed convincingly using de-ionized water, dried by spreading in the laboratory at room temperature [5]. The dry peels were ground to powder and 100 g of the powder was soaked in 10,000 mL absolute ethanol at room temperature. Filtrate was concentrated and dried to powder at 35 °C while the air-dried residue was weighed to evaluate extract yield. The extract was labelled Et-ACPE and stored in laboratory cupboard at room temperature for future use.

2.2 Characterization of extract

The elemental composition on the surface of the extract was determined by energy dispersive X-ray spectroscopy (EDS). Absorbance and wavelengths of absorption were measured by UV–Visible spectroscopy within 400–800 nm range. The active functional groups in the extract were also characterized by FTIR.

2.3 Preparation of silver nanoparticles

The extract was initially prepared into 1000 ppm concentration. 500 mL of 1000 ppm Et-CPE was mixed with 1000 mL of 1 mM AgNO₃ at 25–30 °C, stirred regularly and observed for firm colour change which indicates complete bio-reduction and formation of nanoparticles (NPs). The nanoparticles obtained were designated as Et-AgNPs. Aliquot of the NPs was washed three times in distilled water, dried in oven at 35 °C and used for further analyses while the remaining colloidal solution was stored in amber coloured reagent bottle inside laboratory cupboards at room temperature.

2.4 Characterization of NPs

Formation of plasmon was investigated by UV–Vis spectroscopy. Colloidal properties of the NPs were analysed by DLS in comparison with the crude extracts. X-ray diffraction (XRD) spectroscopy was used to investigate the crystallographic properties of the NPs at $2\theta = 10^\circ\text{--}90^\circ$, also in comparison with the extract. The morphology and size of the NPs was characterized by SEM and TEM. EDS was used to probe and compare the elemental composition of both the extract and NPs. FTIR spectroscopy was also employed to characterize the functionalities in the synthesized NPs within 400–4500 cm⁻¹. The models of equipment used for analyses are shown in supplementary file (SF-1).

2.5 Preparation of steel specimens

Owing to its extensive application especially in the construction of pipelines in oilfield, X80 steel (description in SF-2) was used for the study. Coupons were pre-treated in absolute ethanol to remove grease and lubricants, then polished using SiC abrasives and finished to mirror surface using 2000 grade [5]. Coupons were cleaned with absolute ethanol, dipped in acetone to air-dry and immersed in the prepared test solutions. Coupons for electrochemical experiments were soldered to copper wire and 1 cm² of the polished surface was exposed while the rest were insulated using epoxy adhesives [5].

2.6 Preparation of corrosion test solutions

The blank corrodent was 1.0 M HCl prepared by dilution of analytical grade 37% HCl (description in SF-2) in de-ionized water. Different weights (mg) of the dried Et-ACNPs were

dissolved in fixed concentration (1 L) of 1 M HCl to obtain different concentrations (100–500 mg/L) of Et-AgNPs. As control and basis for comparing the extracts with NPs, 500 mg/L of dried Et-ACPE was also prepared by dissolving same in 1 M HCl. Before addition of the inhibitor, the pH of 1 M HCl was around zero. This pH value did not change even on addition of the inhibitors. Also, both the extract and NPs were highly soluble in the 1 M HCl solution.

2.7 Electrochemical measurements

The potentiostat/galvanostat was assembled (model and assembly in SF-1) and with the test solutions standing for 30 min to corrode the steel, stabilize the open circuit potential (OCP) before actual measurement [5, 30]. The input experimental parameters were as follows: frequency range = 100 kHz–10 mHz for electrochemical impedance spectroscopy (EIS), voltage range = -0.15 V– $+0.15$ V vs. OCP and scan rate = 0.2 mV/s for potentiodynamic polarization (PDP), frequency pair = 2 Hz and 5 Hz; base frequency = 0.01 Hz and amplitude = 10 mV for electrochemical frequency modulation (EFM) and $E_{corr} = \pm 10$ mV and scan rate = 0.25 mV/s for linear polarization resistance (LPR) at room temperature (30 ± 2 °C) [5]. Gamry E-Chem software was used to analyse data obtained to acquire associated electrochemical parameters. Inhibition efficiency was assessed for EIS (I_{EIS}), PDP (I_{PDP}), LPR (I_{LPR}) and EFM (I_{EFM}) using Eqs. 1, 2, 3 and 4, respectively.

$$I_{EIS} = 100 \left(\frac{R_{cti} - R_{ctb}}{R_{cti}} \right) \quad (1)$$

$$I_{PDP} = 100 \left(1 - \frac{i_{corr}^i}{i_{corr}^b} \right) \quad (2)$$

$$I_{LPR} = 100 \left(\frac{R_{pi} - R_{pb}}{R_{pi}} \right) \quad (3)$$

$$I_{EFM} = 100 \left(1 - \frac{i_{corr}^i}{i_{corr}^b} \right) \quad (4)$$

where R_{ctb} and R_{cti} represent charge transfer resistance without and with inhibitor, respectively, i_{corr}^b and i_{corr}^i represent corrosion current density without and with inhibitor, respectively R_{pi} and R_{pb} represent resistance polarization with and without inhibitor, respectively [5].

2.8 Weight loss measurement

X80 steel coupons (dimension 3 cm \times 3 cm \times 0.5 cm) were weighed, immersed by suspension method in 100 mL of

blank and inhibitor (crude extracts and NPs) test solutions and sealed to exclude air. The containers were placed in water bath equilibrated to 30 °C for 6 h after which they were retrieved and cleaned using ASTM procedures [31] and re-weighed; loss in weights were recorded. Triplicates of experiments were conducted and the mean weight loss (Δw) was used to compute corrosion rate (CR , mmpy) according to Eq. 5 [5].

$$CR = \frac{87600 \Delta w}{\rho A t} \quad (5)$$

where ρ , A and t represent density (gcm^{-3}), surface area (cm^2), and immersion time (h), respectively. Corrosion inhibition efficiency (I_w , %) was elucidated using Eq. 6.

$$I_w = 100 \left(1 - \frac{CR_{inh}}{CR_{HCl}} \right) \quad (6)$$

where CR_{HCl} and CR_{inh} represent corrosion rate in the 1 M HCl without inhibitor and with inhibitor, respectively. Similar measurements were replicated at 40 , 50 and 60 °C.

2.9 Surface and corrosion products

Surface deposits on the steel coupon after immersion was mechanically peeled off and analysed by FTIR. Elemental composition, surface morphologies, topographies and other surface features of the retrieved steel coupons in both uninhibited and inhibited solutions were investigated by EDS, SEM and AFM as previously described [29].

3 Results and discussions

3.1 Yield of extracts

The extraction occurred very fast in ethanol and the weight of the residue after drying was found to be 6.7824 g. This means that 3.2176 g of the phytochemicals dissolved at room temperature and was actually recovered in ethanol. This corresponds to a yield of 32.2% . The intensity of the red colour that initially characterized the powdered peels was found to reduce (in the residue) implying that most of the extractable compounds were sufficiently extracted.

3.2 Formation and characterization of NPs in comparison with extract

The formation of NPs was signalled by a change in colour of the mixtures. The colours changed from pale red to reddish brown as shown in Fig. 2, signifying the completion of bio-reduction of the silver ions. The formation of Et-AgNPs occurred within 85 min. Usually, the time taken

for NPs formation varies from extract to extract even with the same metal ion due to differences in chemical natures and concentrations of the phyto-compounds present and on reaction conditions such as temperature and pH [15]. Since formation of the NPs occurred fast, it was not necessary to vary the above conditions because of the intended application. The final colour of NPs solution remained unchanged even after being observed for additional 24 h later. Also, the obtained solution was homogeneous without any sediments, indicating that the AgNPs were highly soluble.

3.2.1 UV-Vis spectroscopy

The UV-Vis spectra of Et-ACPE and the corresponding Et-AgNPs are displayed in Fig. 3a. Actually, the spectrum of

the solution was obtained at 10 min interval but only the initial and final spectra are reported. Formation of NPs produced plasmon resonance absorption band at a different wavelength and absorbance value from that of the pure extract. On complete bio-reduction of the Ag^+ ions, plasmon absorption was observed at $\lambda_{max} = 435$ nm, whereas Et-ACPE absorption occurred at $\lambda_{max} = 510$ nm. Within the range of the broad absorption of Et-ACPE (475–625 nm), it was observed that the NPs showed no change in absorbance values. Most plant extract mediated silver nanoparticles reported in literature show plasmon absorption around 400–500 nm as obtained in this study, and this range has been reported to be characteristic of typical Ag plasmon [30, 31], which supports formation of Et-AgNPs.

3.2.2 XRD spectroscopy

XRD diffraction pattern of the pure extract and the NPs obtained is shown in Fig. 3b. It can be observed that the spectrum of Et-ACPE has neither distinct peaks nor diffraction angles whereas the spectrum of Et-AgNPs show up to four (4) main peaks. The diffraction pattern obtained for Et-ACPE matrix can be attributed to its amorphous nature (hence diffraction of glass) and absence of metallic crystal. However, peaks in the spectrum for Et-AgNPs were obtained at $2\theta = 38.01^\circ$, 45.82° , 64.38° , and 77.45° . To confirm whether the obtained peaks and diffraction angles correspond to reference (standard) values for silver crystal structure, the spectra were analysed using X-PERT HighScore Plus software package (PANalytical) [5]. Results confirm that these peaks correspond to 110 ($2\theta = 38.01^\circ$), 220 ($2\theta = 45.82^\circ$), 220 ($2\theta = 64.38^\circ$) and 311 ($2\theta = 74.45^\circ$) Bragg crystallographic planes of face centre cubic (FCC) structure. The sharpness of all the peaks (without broadening) indicates that NPs are devoid of defects in their crystal structure. The standard reference values of 2θ for silver



Fig. 2 Colour of **a** 20 mL Et-ACPE/100 mL H₂O and **b** 20 mL ACPE/100 mL AgNO₃ (Et-AgNPs) after three hours of formation of NPs

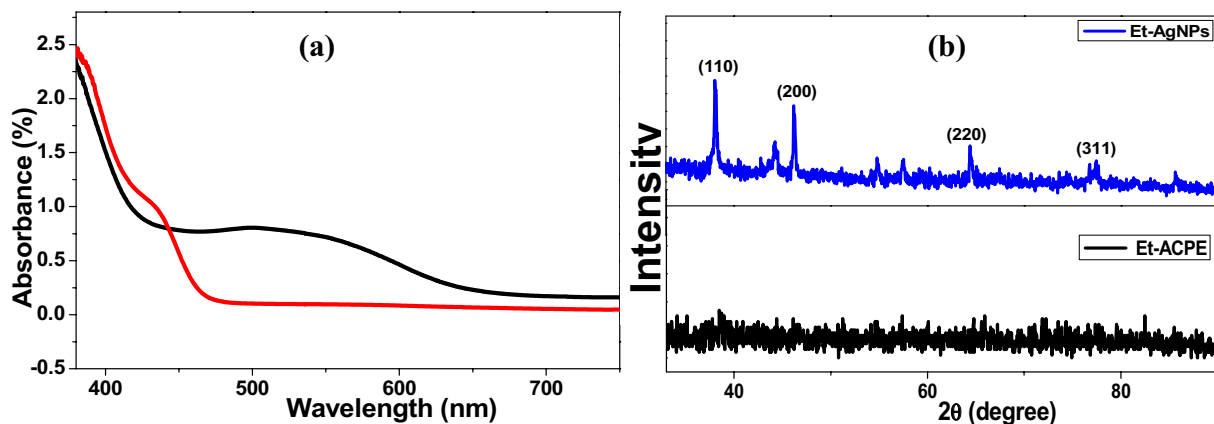


Fig. 3 **a** UV-Vis spectra of Et-ACPE (black) and Et-AgNPs (red) from ACPE. **b** X-ray diffraction pattern of Et-ACPE and Et-AgNPs from ACPE

nanoparticles are 38.162° , 44.597° , 64.674° and 77.544° [34]. XRD results also confirmed the existence of silver in the Ag^0 phase in the NPs. Results of analyses also show that the Ag atoms in the fcc structure with $a=b=c=4.0968 \text{ \AA}$ and $\alpha=\beta=\gamma=90^\circ$, contain cells with volumes $72.43 \times 10^{-6} \text{ pm}^3$ and density (ρ) 10.18 gcm^{-3} . Peak intensity was very high at $2\theta=38.01^\circ$ implying that the preferred orientation of Et-AgNPs is the (111) plane [32, 33].

3.2.3 SEM/EDS

To further confirm that NPs were formed, and to elucidate the shapes of the NPs, SEM images of morphologies of both Et-ACPE and Et-AgNPs were obtained as shown in Fig. 4 (top). It was necessary to select a higher magnification for the NPs to be visible because of their small sizes. Also, the elements composing the surfaces were detected by obtaining EDS spectra of the extract and NPs surfaces as also shown in Fig. 4 (bottom). SEM results also confirmed the amorphous and crystalline morphology of Et-ACPE and Et-AgNPs, respectively. The NPs were spherical in shape and did not agglomerate or aggregate, although some traces of uncapped phyto-compounds were visible

around the surface of the NPs. Other authors have also reported similar observations [34, 35].

EDS scan at the spots corresponding to the extract and particles surfaces reveal that only Et-AgNPs contained silver. Bio-reduction of Ag^+ ions by Et-ACPE is associated with capping of the phyto-compounds on silver. Consequently, the amount of C (atom %) on the NPs surface decreases from 70.12% to 46.54% whereas the amount of surface O (atom %) increases from 27.65 to 36.81%. There was no significant increase in the amount of N atoms—which was found to be 2.23% to 2.25% for Et-ACPE and Et-AgNPs respectively. The amount of Ag (atom %) composing the Et-ACPE and Et-AgNPs was 0% and 14.40% showing that Ag atoms were incorporated into the matrix to form AgNPs. Since O sites are rich in electron cloud, it can be predicted that the NPs surface would exhibit greater electron cloud than the extracts. Greater electron cloud due to more O sites would increase the adsorptive capacity of the NPs compared to the extracts. This presents great prospects for the synthesized nanoparticles to find application in adsorption related phenomena such as removal of heavy metals, corrosion and scale inhibition, and as adsorbents for water treatment, which we are still investigating.

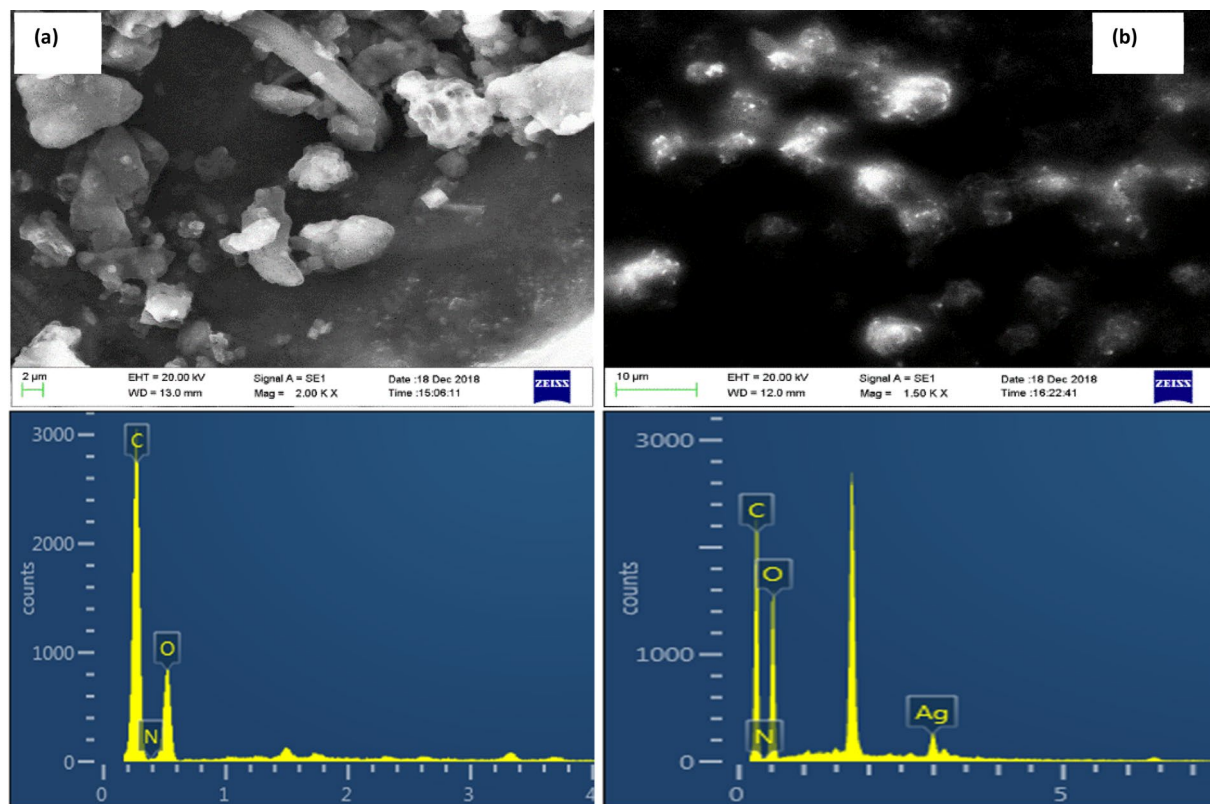


Fig. 4 Top: SEM images of morphologies and; Bottom: EDS profiles of elemental composition of dried **a** Et-ACPE and **b** Et-AgNPs as observed by SEM

3.2.4 TEM

The NPs size and morphology were checked by transmission electron microscopy, TEM (Fig. 5a). It can be implied from results that non-aggregated nanoscale particles of almost non-uniform shapes and sizes were formed. The particles were predominantly spherical in shape and distributed between 20 and 50 nm in size. This size is comparable to those reported for other phyto-mediated silver nanoparticles [16]. However, the size of biosynthesized NPs is usually influenced by some factors such as concentrations of the extract and AgNO_3 , pH, incubation time and volume of extract. Around the nanoparticles, some organic-based materials from the uncapped extracts were also seen just as in SEM/EDS results.

3.2.5 DLS

The zeta potential, polydispersity index, hydrodynamic size and size distribution were obtained via DLS measurements. Average zeta potential of the colloidal NPs determined with alcohol as dispersant was found to be -46.2 ± 0.2 mV. The high magnitude of this zeta potential points to high degree of Coulombic or electrostatic repulsion between highly negatively charged adjacent nanoparticles in the colloidal dispersion which enhances stabilization of the NPs and prevents agglomeration [36, 37]. Although the value obtained is comparably higher than some other plants mediated silver nanoparticles previously reported, it is an indication that the colloidal NPs were highly electrically stabilized, hence highly resistant to aggregation. A higher proportion of the particles were found to be distributed around 78–86 nm hydrodynamic size (Fig. 5b), slightly larger than sizes obtained by TEM analyses but still within the range for nanoparticles. The difference in the size measured by TEM and DLS is indicative of agglomeration state: agglomerated particles will

show much larger sizes by DLS than TEM measurements [38]. However, similar or slightly larger particle sizes from DLS than TEM measurements show that the particles did not agglomerate. In addition, the average polydispersity index (PDI) value was 0.38 indicating that the NPs are almost monodisperse and very stable [39].

3.2.6 FTIR

The FTIR spectrum of the Et-AgNPs was similar to that of Et-ACPE (Fig. 6) but with slight shifts in wave numbers of the absorption peaks, which is characteristic of most plant mediated silver nanoparticles⁴⁰. For the extracts, prominent peaks were observed at 710, 1050, 1350, 1620, 2930 and $3300\text{--}3500\text{ cm}^{-1}$. However, for the NPs, these peaks were found at 680, 1120, 1400, 1650, and 3440 cm^{-1} . The peak at 2930 cm^{-1} which may be assigned to either -CH_2 or C-CH_3 stretching vibrations were found to have disappeared on formation of the NPs. Instead of the broad peak between 3300 and 3500 cm^{-1} obtained with the extract, the NPs produced a sharp intense peak at 3440 cm^{-1} [40]. The broad peak represents intermolecular hydrogen bonded -OH stretching vibrations but can also represent -N-H stretching vibrations. N-H stretching vibrations usually produce a sharp single intense peak at $3300\text{--}3500\text{ cm}^{-1}$ as obtained in the spectrum of the NPs. However, EDS analyses earlier showed that there were no N atoms on the NPs surface and previous HPLC-MS had shown that major compounds in Et-ACPE contain more of -OH group [41], hence this peak can be solely assigned to -O-H vibrations. The peak at 1650 cm^{-1} can be due to C=O stretching in carboxylic acids or stretching vibrations due to non-conjugated C=C moiety. Also, C-O stretch in lactam, N-H amine, C=C stretching in cyclic alkenes or α, β -unsaturated ketones can give rise to the peak at 1650 cm^{-1} . In the fingerprint region, The peak at 1400 cm^{-1} represents C-O stretching vibrations; the one

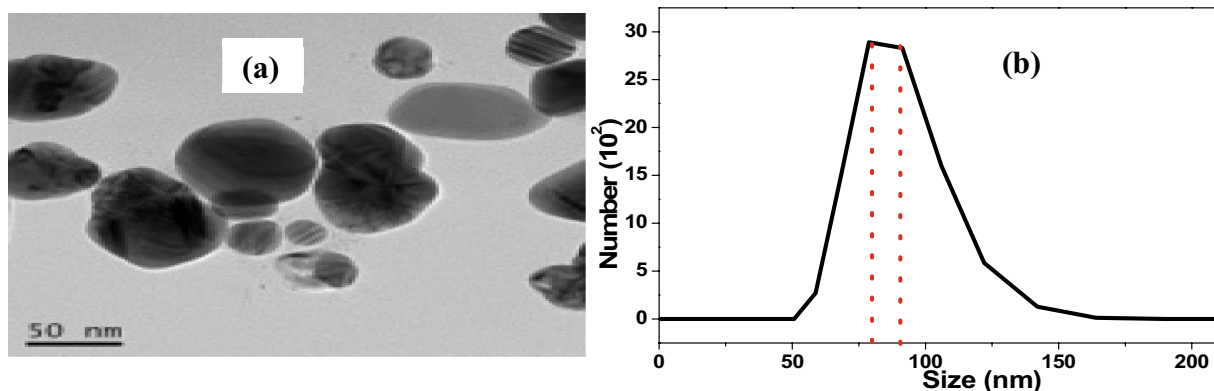
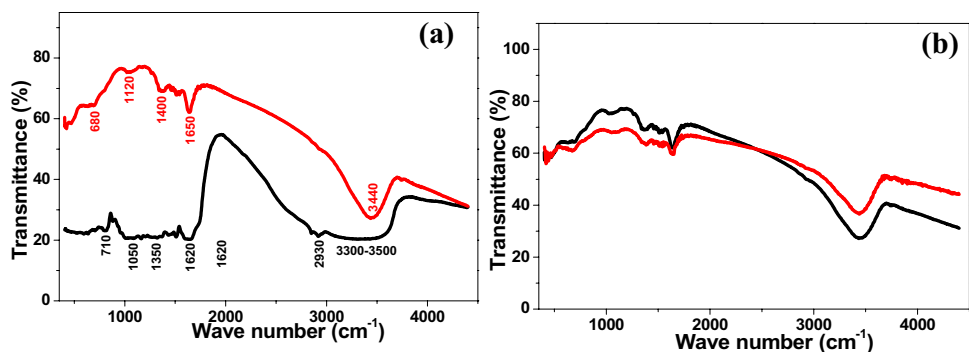


Fig. 5 **a** TEM images of Et-AgNPs and **b** Distribution of hydrodynamic size of Et-AgNPs by DLS intensity measurement

Fig. 6 **a** FTIR spectra obtained for Et-ACPE (black) and Et-AgNPs (red); **b** FTIR spectra obtained for pure Et-AgNPs (black) and surface adsorbed Et-AgNPs (red) on X80 steel



at 1050 cm^{-1} can be assigned to C–OH vibrations of secondary cyclic alcohols while the peak at 710 represents -CH out of plane bending vibrations in ethylenic systems, especially -CH=CH- [5, 42] and was found to have been involved in interaction with silver ions.

3.3 Corrosion studies

3.3.1 EIS

This measurement was performed to probe how addition of the NPs influences the corrosion process, its mechanism

and capacitive response at the steel-acid interface. The OCP was found to stabilize within 450 s (Fig. 7a) indicating corrosion measurements can be accurately taken. However, with respect to the blank acid, OCP shifts to positive values in the presence of the inhibitors. Based on this observation, the additives may be considered as being anodic inhibitor. Impedance data obtained were used to construct Nyquist plots shown in Fig. 7b and the plots were analysed by fitting using a simple CPE equivalent circuit model shown in Fig. 7c which afforded good fitness in the order of 10^{-4} . The obtained EIS parameters are displayed in Table 1. All the plots (both the blank and

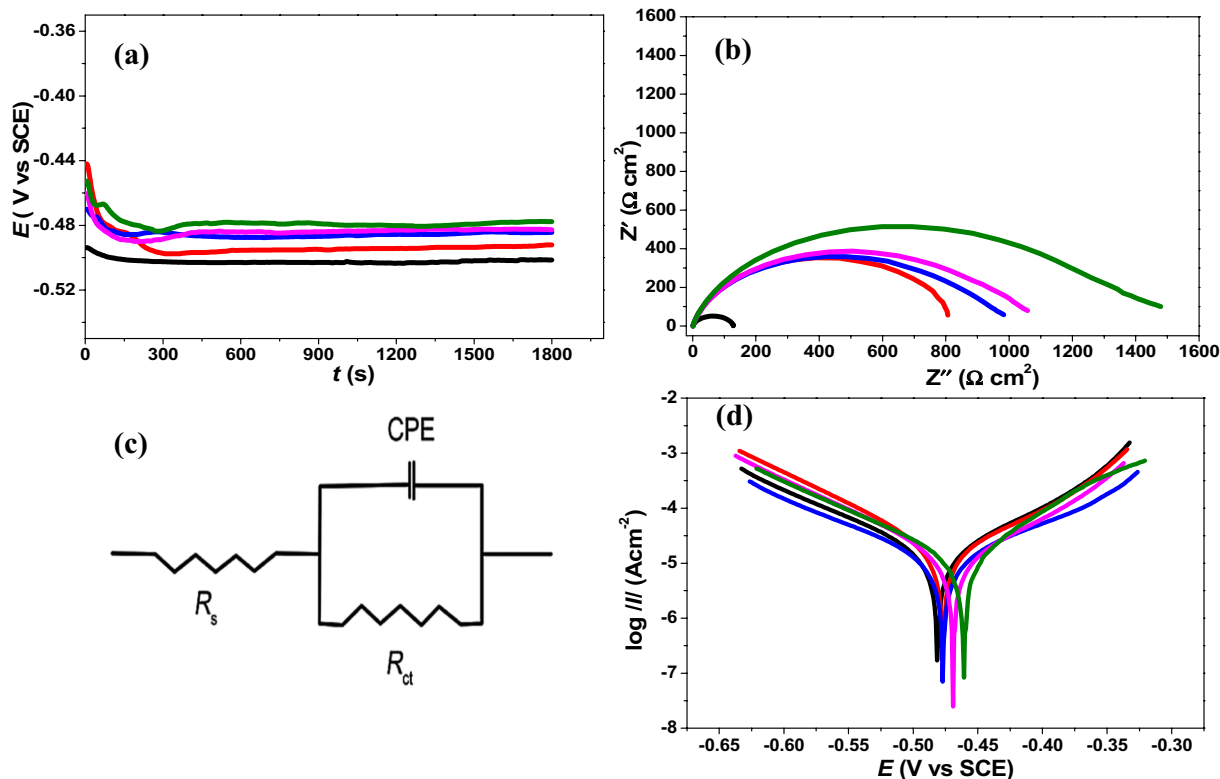


Fig. 7 **a** OCP vs time plot **b** Nyquist plot and **c** Equivalent circuit used to fit data and **d** Tafel plot for the corrosion of X80 steel in blank 1 M HCl and 1 M HCl inhibited using Et-ACPE and Et-AgNPs.

Key: Black= 1 M HCl; red=500 mg/L Et-ACPE; blue=100 mg/L Et-AgNPs; purple=200 mg/L Et-AgNPs; green=500 mg/L Et-AgNPs)

the inhibited solutions) yielded single semicircles indicating that single charge transfer process occurred at the interface. Similarity in shape of the semicircles also indicates similar corrosion mechanism despite addition of the inhibitors. Thus, addition of inhibitors has no significant influence on the corrosion mechanism of X80 steel in 1 M HCl solution. As the concentration of NPs was increased, both charge transfer resistance and inhibition efficiency increased in magnitude. The magnitude of the calculated double layer capacitance (C_{dl}) was highest in the blank acid solution, and decreased with increase in Et-AgNPs concentration. This is a consequence of increase in the local dielectric constant or insulation property at the interface due to inhibitor adsorption²⁹. Also, as concentration of the NPs increases, C_{dl} decreases, the insulating effect of the surface layer increases due to increased adsorption of more Et-AgNPs.

3.3.2 PDP

Tafel plots (Fig. 7d) were constructed from polarization data and the effect of addition of different concentrations of the NPs on the cathodic and anodic half reactions was investigated. Addition of the NPs decreased the corrosion current density (I_{corr}), and consequently, the corrosion rate. The obtained I_{corr} values (Table 2) decreased as concentration of NPs increased, and the Tafel slopes were also altered. Increasing the Et-AgNPs concentration also resulted in higher inhibition efficiency and the magnitude and trend of efficiency was similar and comparable to EIS results. For all the nanoparticles solutions, the slopes of the anodic branches and the corresponding anodic Tafel constant (β_c) values were highly displaced compared to those of the cathodic branches and constants (β_a). This establishes that the NPs has dominating effect or impact

on anodic than cathodic reaction [29]. It was also observed that E_{corr} values shift towards more positive values, also depicting dominant anodic influence and thus supporting the trend of the Tafel constants. Based on these observations, it could be implied that Et-AgNPs influences more of the anodic reaction than cathodic reaction. This trend is in agreement with OCP measurement. However, since the displacement in E_{corr} values is less than 0.85 V, the NPs can be categorized as mixed type inhibitor with anodic predominance [43–45].

3.3.3 EFM

EFM measurement afforded complementary results to EIS and PDP and to further afforded corrosion current values via small signals. The efficiency of corrosion inhibition (Table 3) was computed from the corrosion current values. As obtained with impedance and polarization measurements, inhibition efficiency increased as NPs concentration increased. Furthermore, causality factors, CF-2 and CF-3 were obtained and all the values were approximate to theoretical values of 2 and 3 respectively, indicating good quality of measurements [46, 47]. The Tafel constants (β_a and β_c) constants were also obtained, and as observed in PDP results, there was more spread in β_a than β_c values, supporting more impact on the anodic than cathodic half reaction.

3.3.4 LPR

LPR experiment was carried out to further support the inhibition efficiency obtained from prior electrochemical measurements. The Stern-Geary equation (Eq. 7) was used to estimate polarization resistance, and used to compute inhibition efficiency.

Table 1 EIS parameters for the inhibition of X80 steel corrosion in 1 M HCl containing Et-ACPE and different concentrations of its Et-AgNPs

Test solution	$R_s(\Omega)$	$R_{ct}(\Omega)$	n	$C_{dl}(\mu Fcm^{-2})$	$I_{EIS}(\%)$	$\chi^2 10^{-4}$
Blank	0.864 ± 0.012	128.8 ± 1.3	0.844	26.72	–	1.08
500 mg/L ACPE	0.918 ± 0.018	800.2 ± 3.8	0.846	11.04	83.9 ± 1.1	1.07
100 mg/L AgNPs	1.024 ± 0.021	1070.6 ± 5.7	0.857	5.13	88.0 ± 1.7	3.11
200 mg/L AgNPs	1.108 ± 0.016	1187.9 ± 9.6	0.863	2.02	89.2 ± 1.6	3.09
500 mg/L AgNPs	1.241 ± 0.011	1576.4 ± 11.4	0.881	0.74	91.8 ± 2.2	2.94

Table 2 PDP parameters for the inhibition of X80 steel corrosion in 1 M HCl containing Et-ACPE and different concentrations of its Et-AgNPs

Test solution	$I_{corr}(Acm^{-2})$	$E_{corr}(V)$	$\beta_a(mVdec^{-1})$	$\beta_c(mVdec^{-1})$	$I_{PDP}(\%)$
Blank	996.1 ± 2.8	−0.489 ± 0.006	151.4	−144.7	–
500 mg/L ACPE	176.8 ± 1.6	−0.480 ± 0.005	141.3	−140.2	82.3 ± 1.5
100 mg/L AgNPs	142.4 ± 2.1	−0.476 ± 0.004	130.8	−138.6	85.7 ± 1.3
200 mg/L AgNPs	124.1 ± 0.8	−0.468 ± 0.007	118.4	−135.2	87.5 ± 1.2
500 mg/L AgNPs	80.7 ± 1.2	−0.460 ± 0.008	102.6	−128.1	91.9 ± 1.3

Table 3 EFM parameters for the inhibition of X80 steel corrosion in 1 M HCl containing ACPE and different concentrations of its Et-AgNPs

Test solution	β_a (mVdec. ⁻¹)	β_c (mVdec. ⁻¹)	CF – 2	CF – 3	I_{corr} (Acm ⁻²)	I_{EFM} (%)
Blank	133.8	-112.7	2.011	2.962	861.3 ± 4.4	-
500 mg/L ACPE	121.4	-109.9	1.992	3.011	162.4 ± 1.7	81.1 ± 1.3
100 mg/L AgNPs	107.2	-106.1	1.996	2.984	141.7 ± 1.6	83.5 ± 1.2
200 mg/L AgNPs	94.8	-104.8	1.981	2.976	106.5 ± 0.8	87.6 ± 1.2
500 mg/L AgNPs	91.6	-97.6	1.968	3.004	64.3 ± 1.1	92.5 ± 1.4

Table 4 LPR parameters for the inhibition of X80 steel corrosion in 1 M HCl containing ACPE and different concentrations of its Et-AgNPs

Test solution	R_p (Ω)	I_{PDP} (%)
Blank	104.2 ± 3.1	-
500 mg/L ACPE	558.4 ± 4.7	81.3 ± 2.4
100 mg/L AgNPs	639.6 ± 5.2	83.7 ± 1.6
200 mg/L AgNPs	784.1 ± 4.2	86.7 ± 1.1
500 mg/L AgNPs	1189.4 ± 13.6	91.2 ± 1.2

$$R_p = \frac{\beta_a \beta_c}{2.303 I_{corr} (\beta_a + \beta_c)} \tag{7}$$

The R_p and inhibition efficiency values obtained (Table 4) also increased as NPs concentration increased, similar to trends obtained for other measurements. Also, polarization resistance increases with the solutions inhibited by the NPs than the crude extract supporting that adsorption of the NPs resulted in increased resistance around the electrode surface, depicting increased surface insulation. The results obtained for LPR also follow similar trend as other EIS, PDP and EFM measurements.

3.3.5 Weight loss

Loss in weight and corrosion rate of X80 steel coupons in the blank 1 M HCl and containing both Et-ACPE and Et-AgNPs were measured by weight loss experiments and results were compared. The obtained data of weight loss and corrosion rate are presented in Table 5. Weight loss,

and consequently corrosion rate, was highest in the blank acid solution, but reduced on addition of the extract and NPs. In comparison, the NPs offered higher inhibition efficiency and were more thermally stable than the crude extracts. Thus, an equivalent concentration of the NPs was more efficient than Et-ACPE at all temperatures studied (see Table 5). In fact, a very low concentration of the NPs (100 mg/L) exhibited higher efficiency than 500 mg/L Et-ACPE. This demonstrates that processing the extract into NPs enhances their anticorrosion behaviour, perhaps due to improved adsorption capacity and the presence of more electron cloud around O atoms (according to EDS results) for adsorption on the steel surface. Efficiency of inhibition increases as NPs concentration increases and was fairly stable at as temperature increases compared to the extract. In terms of pH, addition of the extract and nanoparticles to a fixed volume of 1 M HCl did not influence the pH of the test solutions. Thus, it may be considered that the acid remained in the live form even in the presence of the additives. This also implies that the additives did not reduce or increase the acidity of 1 M HCl.

3.3.6 Kinetics, thermodynamics and adsorption mechanistic studies

Like most chemical reactions, the rate of corrosion increases as temperature increases. The presence of the NPs reduced corrosion rate of X80 steel. Corrosion rate data was used to construct linearized plots shown in Fig. 8a and b based on Arrhenius equation (Eq. 8) and transition state equation (Eq. 9), respectively [48, 49].

Table 5 Weight loss, corrosion rate and inhibition efficiency of Et-ACPE and Et-AgNPs against X80 steel corrosion in 1 M HCl at 30 – 60 °C

Test solution	30 °C			40 °C			50 °C			60 °C		
	Δw (g)	CR mmpy	I_w (%)	Δw (g)	CR mmpy	I_w (%)	Δw (g)	CR mmpy	I_w (%)	s (g)	CR mmpy	I_w (%)
Blank	0.0563	12.22	-	0.0864	18.74	-	0.1402	30.41	-	0.2363	51.18	-
500 mg/L ACPE	0.0104	2.26	81.5 ± 1.2	0.0188	4.07	78.3 ± 0.6	0.0356	7.72	74.6 ± 1.1	0.0717	15.56	69.6 ± 1.3
100 mg/L AgNPs	0.0091	1.98	83.8 ± 0.9	0.0169	3.67	80.4 ± 0.6	0.0320	6.93	77.2 ± 0.8	0.0592	12.85	74.9 ± 1.1
200 mg/L AgNPs	0.0072	1.56	87.2 ± 0.6	0.0119	2.59	86.2 ± 0.4	0.0227	4.93	83.8 ± 0.6	0.0493	10.70	79.1 ± 0.9
500 mg/L AgNPs	0.0036	0.78	93.6 ± 0.7	0.0075	1.63	91.3 ± 0.7	0.0155	3.37	88.9 ± 1.2	0.0373	8.09	84.2 ± 0.8

$$\log CR = \log Z - \frac{E_a}{2.303RT} \quad (8)$$

$$\log \left(\frac{CR}{T} \right) = \left[\left(\log \left(\frac{R}{Nh} \right) + \left(\frac{\Delta S^*}{2.303R} \right) \right) \right] - \left(\frac{\Delta H^*}{2.303RT} \right) \quad (9)$$

where CR is the corrosion rate, Z the Arrhenius pre-exponential or frequency factor, R is the universal gas constant, N is Avogadro's number, T is absolute temperature, ΔH^* and ΔS^* is the enthalpy and entropy change of activation respectively [45].

Activation energy was determined from the Arrhenius plots while enthalpy and entropy changes were deduced from transition state plots. Results reveal that activation energy was lowest in the free acid medium and increased on addition and with increasing Et-AgNPs concentration (Table 6). The activation energy obtained with the blank acid solution could be considered as the minimum energy with which the acid molecules must generate for effective collision on the steel surface to cause its corrosion. Therefore, in the presence of the NPs, the collision of the acid molecules with the steel surface acid must generate higher energy than with the blank, hence corrosion inhibition. Addition of the NPs increase this minimum energy or energy barrier and limits the number of successful collisions that could have resulted to corrosive attack. This trend of activation energy is often associated with physical adsorption mechanism involving electrostatic interaction of charged inhibitor groups with charged species on steel surface [50, 51]. Adsorption of NPs on X80 steel surface was found to be exothermic and resulted in decrease in entropy of the solution, similar to other steel corrosion inhibitors [5].

The mechanism of adsorption of the NPs on the steel surface and subsequent corrosion inhibition was studied by means of adsorption isotherms. The surface coverage data for various concentrations (mg/L) of Et-AgNPs were used to plot various adsorption isotherms but the

Table 6 Activation parameters for the inhibition of X80 steel corrosion in 1 M HCl containing different concentrations of Et-AgNPs

Test solution	E_a (kJmol ⁻¹)	A ($\times 10^9$)	$-\Delta H$ (kJmol ⁻¹)	ΔS (kJmol ⁻¹)
Blank	39.64	0.08	37.92	0.28
500 mg/L ACPE	40.20	0.05	38.22	0.24
100 mg/L AgNPs	53.60	0.04	39.02	0.23
200 mg/L AgNPs	58.11	0.02	43.48	0.19
500 mg/L AgNPs	63.47	0.01	47.92	0.13

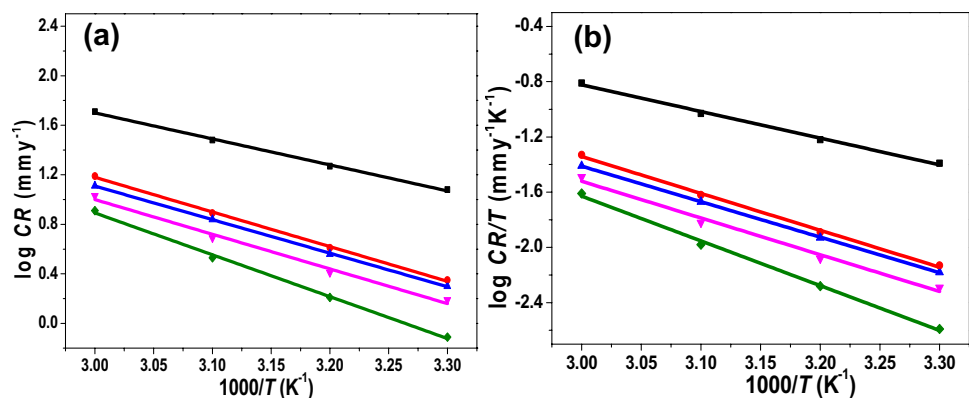
Langmuir isotherm afforded the best fit ($R^2 \geq 0.9995$). The mathematical expression for this model is given in Eq. 10 and can be related with free energy of adsorption (ΔG_{ads}) by Eq. 11 [5].

$$\frac{C_{NPs}}{\theta} = \frac{1}{K_{ads}} + C_{NPs} \quad (10)$$

$$\Delta G_{ads} = -RT \ln 55.5K_{ads} \quad (11)$$

where C_{NPs} is the concentration of the NPs (mg/L), θ is the fractional surface coverage evaluated by multiplying inhibition efficiency by 0.01, K_{ads} is the adsorption-desorption equilibrium constant, R is the universal gas constant and T is the absolute temperature [52]. Values of K_{ads} obtained decreased as temperature increases indicating that the equilibrium shifts in favour of desorption of NPs molecules as temperature increases. Thus, increase in temperature decreases the inhibitor-steel surface binding strength. ΔG_{ads} values were all negative, and between -21.52 kJmol⁻¹ to -34.28 kJmol⁻¹, indicating that adsorption of the NPs occurs spontaneously, just like many other adsorption processes. Also, the values are less negative than -40 kJmol⁻¹ indicating physical adsorption mechanism [53]. This involves basically electrostatic interaction between

Fig. 8 a Arrhenius plot and **b** Transition state plot for the corrosion of steel in 1 M HCl without and with Et-ACPE and Et-AgNPs. Key: Black = 1 M HCl; red = 500 mg/L Et-ACPE; blue = 100 mg/L Et-AgNPs; purple = 200 mg/L Et-AgNPs; green = 500 mg/L Et-AgNPs



charged species in the inhibitor and the steel surface [47]. Since silver in the NPs is zero-valent, this interaction can possibly occur between the phytoconstituents (capped to the silver) and the steel surface. Each particle could be considered to be composed of one or more capped phyto-compounds containing electron rich site(s) such as O and C=C, which can interact with Fe ions on steel surface. Thus, the nanoparticles enhance the adsorption of more capped phyto-compounds on Fe surface resulting in enhanced corrosion inhibition.

3.4 Stability of Et-AgNPs

The stability of the NPs with aging was estimated for 16 weeks of preparation at different temperatures using weight loss measurement. Prior to this, already prepared samples were stored in laboratory cupboards inside reagent bottles at room temperature. The efficiency of the highest concentrations each of Et-AgNps and Et-ACPE were tested by weight loss method every two weeks (from the date they were initially prepared) at the studied temperatures. Results (Fig. 9) show that the efficiency of Et-ACPE started to decline after 6 weeks, but the NPs were still as efficient throughout the period. The decline in efficiency of the extract was worse at 60 °C. This can be explained in terms of ease of thermal and biodegradation: biochemical degradation of the extract could have easily started within this period, whereas the NPs were stable and did not biodegrade within the time under consideration.

3.5 Examination of corrosion products

3.5.1 FTIR

After 6 h of immersion, the retrieved steel coupon was cleaned, air-dried and a thin film observed on its surface was removed by mechanical scrapping and investigated by FTIR. The FTIR spectra of the NPs and the surface film (Fig. 6b) were similar in terms of peak positions and intensity of absorption. This demonstrates that the surface film represents adsorbed Et-AgNPs. Also, since there were only slight changes in peak positions, it can be assumed that there was interaction between the NPs and steel surface, but the adsorptive interaction did not result in the formation of actual chemical bonds. Therefore, the inhibitor-surface interaction can be considered as physical in nature involving either electrostatic interactions between charged species or involving weak van der Waals interactive forces between surface species and inhibitor sites. Such interactions signify physical adsorption mechanism thus supporting earlier predictions made. Slight displacement in the position of the peak around 680 cm^{-1} to 650 cm^{-1} was observed and this could represent complex

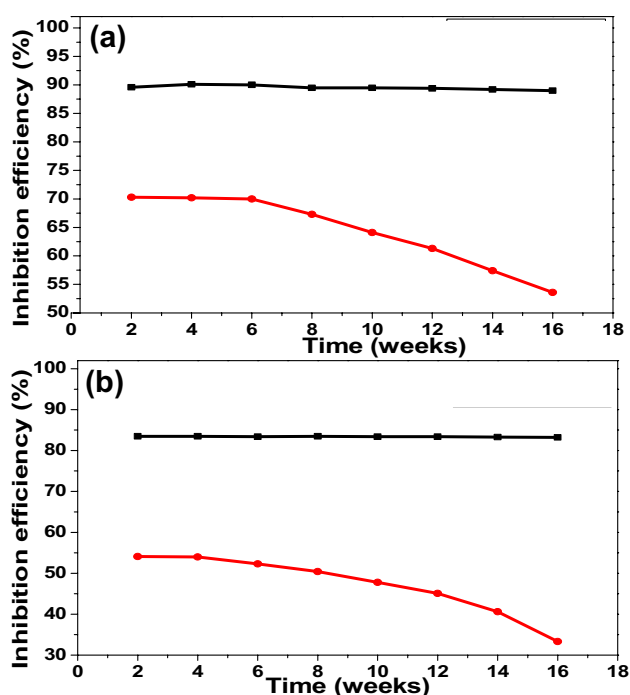


Fig.9 Comparison of inhibition efficiency of 500 mg/L Et-AgNPs (black line) with 500 mg/L Et-ACPE (red line) and their stability with preservation time at **a** 30 °C and **b** 60 °C

interaction between electron rich $\text{C}=\text{C}$ groups on the NPs with d-orbitals of Fe^{2+} on the steel surface, which could be physical in nature.

3.5.2 EDS

The elemental composition of the steel surface after immersion for 6 h in 1 M HCl containing the Et-AgNPs was elucidated and compared with the surface retrieved from the uninhibited acid solution. The scan was conducted with reference to C, N, O, Cl, Ag and Fe atoms only and the obtained EDS profiles are shown in Fig. 10b. It was observed that the steel surface retrieved from the blank acid solution was composed of very high amount of Fe but with no trace of Ag. On addition of Et-AgNPs to the acid, the Fe composition (Wt. %, Atomic %) on the surface retrieved from the inhibited solution decreased from (97.19%, 88.53%) to (93.58%, 83.43%). This may be due to coverage of Fe sites on the surface by some adsorbed species from the inhibitor such as adsorbed Ag (2.45%, 1.13%) and other atoms which could have only come from the inhibitor. The amount of O and C increased from (0.16%, 0.49%) and (2.52%, 10.68%) to (0.76%, 2.28%) and (3.11%, 12.90%) respectively. This implies C and O from the inhibitor were adsorbed on the surface, thereby covering Fe atoms. The amounts of Cl atoms decreased from (0.11%, 0.16%) to (0.08%, 0.11%) supporting replacement

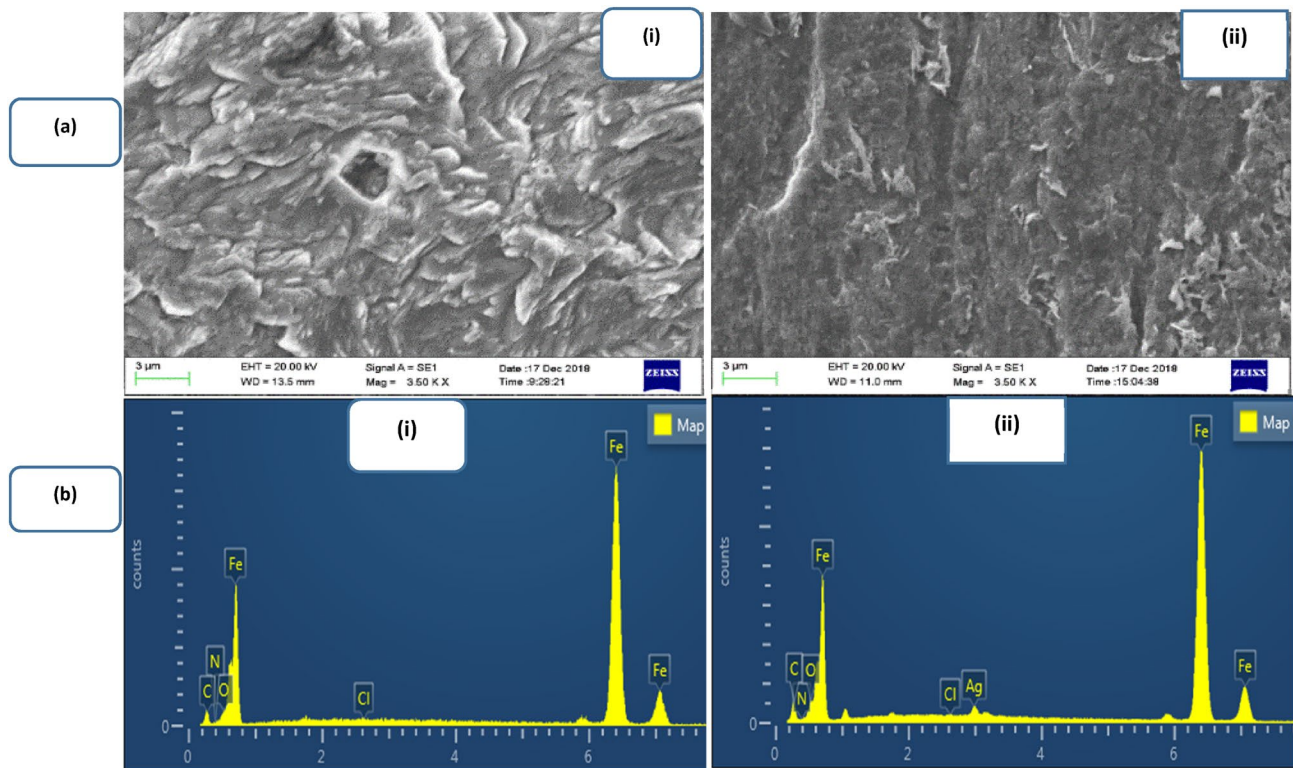


Fig. 10 **a** SEM micrographs and **b** EDS spectra of X80 steel surface retrieved from (i) 1 M HCl solution and (ii) 1 M HCl solution inhibited with 20% Et-AgNPs

of chloride ions with inhibitor species on the surface. Previous EDS investigation using the NPs revealed it contains no N atoms. However, EDS analyses of the steel surface reveals that it was composed of (0.16%, 0.49%) of N before corrosion inhibition and negligible N (0.01%, 0.03%) after inhibition, which removes the possibility of involvement of N in the adsorption process because the observed N could have come from air.

3.6 Morphological examination and surface protection

3.6.1 SEM

X80 steel surfaces retrieved from both uninhibited and inhibited 1 M HCl were observed by SEM and their morphologies are shown in Fig. 10a. When the inhibitor was not added, corrosive attack resulted in severe damage of the surface, but with inhibitor, the surface was reasonably smooth with only slight corrosive damage. This demonstrates that Et-AgNPs has great potential to suppress the corrosion of X80 steel, although it does not stop the corrosion completely. By comparing the morphologies, it can be affirmed that Et-AgNPs shows excellent retarding effect

on the steel corrosion in 1 M HCl solution even within the 6 h contact time.

3.6.2 AFM

The surface features and morphologies of X80 steel surface immersed in 1 M HCl without and with Et-AgNPs also were examined at nano- to micro-scale using AFM [5]. We obtained 3D images of the peaks and pits on the surfaces as well as 2D photos of the amplitude and topography surfaces and these are shown in Fig. 11. It was observed that in the blank solution, extreme surface roughness with many pits and peaks were prevalent, indicating severe damage due to rapid corrosion by the acid. Depths of surface pits and heights of peaks were compared from root mean square (RMS) height parameters data generated from the experiment (Fig. 11(iv)). RMS estimation since is considered to be of high sensitivity to large surface deviations with respect to the mean line [48, 49]. In the absence and presence of Et-AgNPs, the maximum peak heights (S_p) were 547 nm and 200 nm above the mean plane of the surface, respectively, whereas the deepest pits (S_v) were 444 nm and 200 nm below the mean plane of the surface, respectively. These clearly show that deeper pits and higher

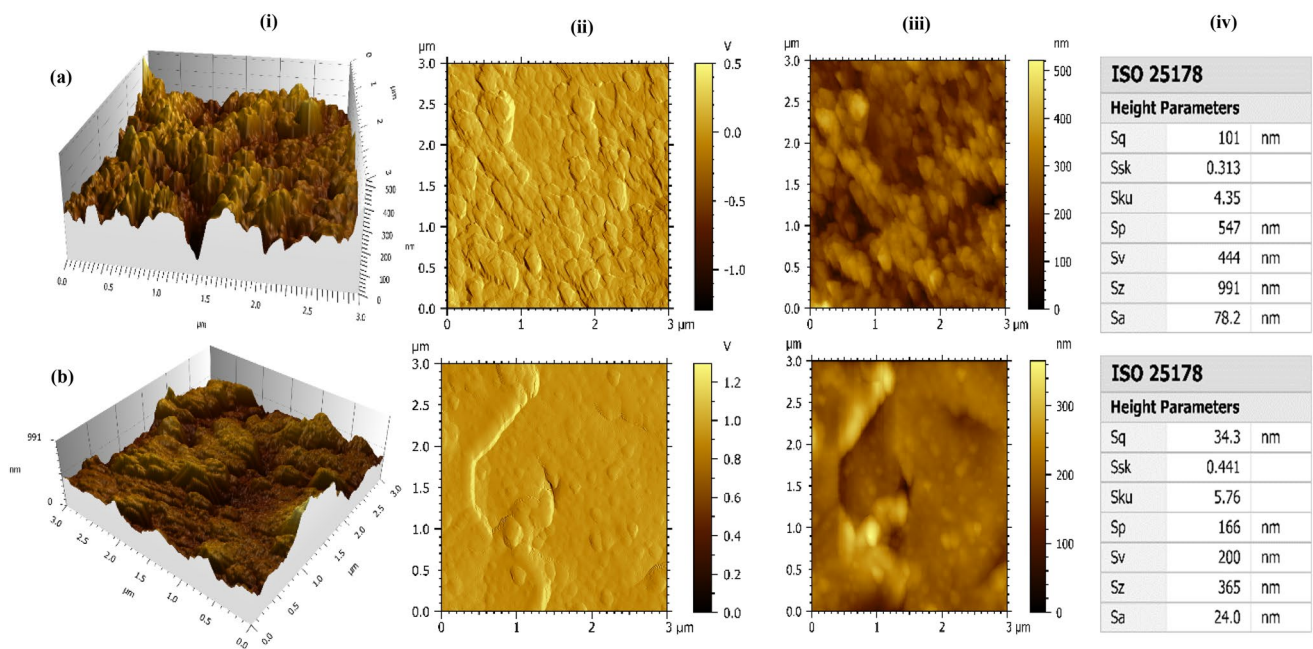


Fig. 11 AFM images of (i) 3D morphology (ii) amplitude (iii) topography and (iv) height parameters for X80 steel surface after immersion in **a** 1 M HCl and **b** 1 M HCl inhibited by Et-AgNPs

peaks were created by corrosive damage due to the blank acid solution than when Et-AgNPs was added [5, 54]. In comparison with the blank acid, addition of Et-AgNPs reduces pitting by about 69.7% and reduces peak heights by 55.0%, which indicates highly efficient anti-corrosion effect.

RMS heights (Sq) were 101 nm and 34.3 nm without and with Et-AgNPs respectively. The magnitude of Sq portrays the standard deviation of peak height at a defined area from the mean plane [29]. Thus, on adding Et-AgNPs, peaks height due to corrosive damage reduced averagely by about 66.0% in comparison with the blank. Skewness parameter ($Ssk < 0$) indicates that height distribution in the presence of inhibitor were more skewed above the mean plane; kurtosis ($Sku > 3$) parameter indicates reduction in spiking of height distribution in the presence of the NPs [29, 54, 55]. Also, the maximum height (Sz) and arithmetic mean height (Sa) attained due to corrosive damage of the surface by the acid was 991 nm and 78.2 nm respectively, but in the presence of the inhibitor, these heights respectively reduced to 365 nm and 24.0 nm corresponding to 63.2% and 69.3% reduction, respectively. The results obtained from AFM studies and all the associated RMS parameters confirm that addition of the Et-AgNPs afforded a relatively smoother steel surface with minimal pits and reduced surface degradation, hence efficient corrosion protection.

3.7 Comparative study

Many corrosion inhibitors derived from plant materials are not stable—they easily degrade in the presence of heat or when stored for long due to actions of biochemical agents. This places limitation on the application of this kind of corrosion inhibitors. Various plant-based corrosion inhibitors have been reported for similar application as the materials reported in this study. For instance, many of such materials have been documented in a recent review [56]. In comparison, ET-AgNPs competes with or performs better than many of such corrosion inhibitors in terms of efficiency. Some examples include Longan peels extract [57], *Musa paradisiaca* (banana) peels extract [58], rice hull extracts [59], watermelon rind extracts [60], *Pisum sativum* peels extracts [61] and *Rollina occidentalis* extract [62]. In addition, Et-AgNPs is also more efficient than nanoparticles composites prepared from olive leaves extract [19] and *Musa paradisiaca* peels extracts [63] which were recently reported in literature.

4 Conclusions

Green silver nanoparticles were synthesized using ethanol extracts of *Allim cepa* peels and silver nitrate, characterized and evaluated as corrosion inhibitor for X80 steel in 1 M HCl. Based on our results, it has been concluded that

Et-AgNPs produces plasmon absorption at 435 nm and its formation occur within 85 min. Et-AgNPs are crystalline with no defects, having a fcc structure with Ag atoms predominantly oriented along (111) plane. Et-AgNPs synthesized are non-aggregating, monodispersed with spherical shapes and particle sizes distributed between the range of 20–50 nm. Et-AgNPs surface contains more O sites which conveys higher adsorptive capacity than the crude extract. The NPs are 89.7% and 83.5% efficient in inhibiting corrosion of X80 steel in 1 M HCl at 30 °C and 60 °C, respectively, and act as mixed type inhibitor with dominant effect on anodic half reaction. Addition of the NPs reduces pits and peaks due to acid corrosive attack by 69.7% and 66.0% respectively, protects steel surface against corrosion. Interaction of the NPs with steel surface results in formation of surface complex facilitated by O sites in the NPs. Et-AgNPs from ACPE is suitable for application as green, inexpensive and efficient alternative corrosion inhibitor for oilfield pickling and cleaning operations.

Acknowledgements Authors are thankful to the financial assistance provided by the National Natural Science Foundation of China (No. 52074232). Also, the authors appreciate the assistance of Ruiyun Li and Ubong Etim during the conduct of the experiments and data analyses.

Declarations

Conflict of interest We declare that there is no conflict of interest among authors.

Open Access This article is licensed under a Creative Commons Attribution 4.0 International License, which permits use, sharing, adaptation, distribution and reproduction in any medium or format, as long as you give appropriate credit to the original author(s) and the source, provide a link to the Creative Commons licence, and indicate if changes were made. The images or other third party material in this article are included in the article's Creative Commons licence, unless indicated otherwise in a credit line to the material. If material is not included in the article's Creative Commons licence and your intended use is not permitted by statutory regulation or exceeds the permitted use, you will need to obtain permission directly from the copyright holder. To view a copy of this licence, visit <http://creativecommons.org/licenses/by/4.0/>.

References

- Mishra A, Shoesmith D, Manning P (2016) Materials selection for use in concentrated hydrochloric acid. *Corros* 73:68
- Goyal M, Kumar S, Bahadur I, Verma C, Ebenso EE (2018) Organic corrosion inhibitors for industrial cleaning of ferrous and non-ferrous metals in acidic solutions: a review. *J Mol Liq* 256:565
- Finšgar M, Jackson J (2014) Application of corrosion inhibitors for steels in acidic media for the oil and gas industry: a review. *Corros Sci* 86:17
- Rani BE, Basu BBJ (2012) Green inhibitors for corrosion protection of metals and alloys: an overview. *Int J Corros*. <https://doi.org/10.1155/2012/380217>
- Ituen E, Singh A, Yuanhua L, Li R (2020) Synthesis and evaluation of anticorrosion properties of onion mesocarp-nickel nanocomposites on X80 steel in acidic cleaning solution. *J Mater Res Technol*. <https://doi.org/10.1016/j.jmrt.2020.01.017>
- Eduok UM, Umoren SA, Udoh AP (2012) Synergistic inhibition effects between leaves and stem extracts of *Sida acuta* and iodide ion for mild steel corrosion in 1 M H₂SO₄ solutions. *Ara-bian J Chem* 5:325
- Krishnaveni K, Ravichandran J (2014) Effect of aqueous extract of leaves of *Morinda tinctoria* on corrosion inhibition of aluminium surface in HCl medium. *Transac Nonferr Metals Soc China* 24:2704
- Jokar M, Farahani TS, Ramezanzadeh B (2016) Electrochemical and surface characterizations of morus alba pendula leaves extract (MAPLE) as a green corrosion inhibitor for steel in 1 M HCl. *J Taiwan Inst Chem Eng* 63:436
- Abrishami S, Naderi R, Ramezanzadeh B (2018) Fabrication and characterization of zinc acetylacetonate/*Urtica Dioica* leaves extract complex as an effective organic/inorganic hybrid corrosion inhibitive pigment for mild steel protection in chloride solution. *Appl Surf Sci* 457:487
- Ramezanzadeh M, Sanaei Z, Bahlakeh G, Ramezanzadeh B (2018) Highly effective inhibition of mild steel corrosion in 3.5% NaCl solution by green Nettle leaves extract and synergistic effect of eco-friendly cerium nitrate additive: Experimental, MD simulation and QM investigations. *J Mol Liq* 25:67
- Loto RT (2018) Surface coverage and corrosion inhibition effect of *Rosmarinus officinalis* and zinc oxide on the electrochemical performance of low carbon steel in dilute acid solutions. *Res Phys* 8:172
- Bahlakeh G, Ramezanzadeh M, Ramezanzadeh B (2017) Experimental and theoretical studies of the synergistic inhibition effects between the plant leaves extract (PLE) and zinc salt (ZS) in corrosion control of carbon steel in chloride solution. *J Mol Liq* 248:854
- Sanaei Z, Shahrabi T, Ramezanzadeh B (2017) Synthesis and characterization of an effective green corrosion inhibitive hybrid pigment based on zinc acetate-*Cichorium intybus* L leaves extract (ZnA-CIL. L): Electrochemical investigations on the synergistic corrosion inhibition of mild steel in aqueous chloride solutions. *Dyes Pigm* 139:218
- Loto RT, Olowoyo O (2018) Corrosion inhibition properties of the combined admixture of essential oil extracts on mild steel in the presence of SO₄²⁻ anions. *South African J Chem Eng* 26:35
- Motamedi M, Ramezanzadeh B, Mahdavian M (2018) Corrosion inhibition properties of a green hybrid pigment based on *Pr-Urtica Dioica* plant extract. *J Indus Eng Chem* 66:116
- Mittal AK, Chisti Y, Banerjee UC (2013) Synthesis of metallic nanoparticles using plant extracts. *Biotechnol Adv* 31:346
- Ahmed S, Ahmad M, Swami BL, Ikram S (2016) A review on plants extract mediated synthesis of silver nanoparticles for antimicrobial applications: a green expertise. *J Adv Res* 7:17
- Ituen E, Ekemini E, Yuanhua L, Li R, Singh A (2020) Mitigation of microbial biodeterioration and acid corrosion of pipework steel using *Citrus reticulata* peels extract mediated copper nanoparticles composite. *Int Biodeterior Biodegrad* 149:104935
- Essien EA, Kavaz D, Ituen EB, Umoren SA (2018) Synthesis, characterization and anticorrosion property of olive leaves extract-titanium nanoparticles composite. *J Adhes Sci Technol* 32:1773
- Idrees M, Batool S, Kalsoom T, Raina S, Sharif HMA, Yasmeen S (2019) Biosynthesis of silver nanoparticles using *Sida acuta* extract for antimicrobial actions and corrosion inhibition potential. *Environ Technol* 40:1071
- Ituen E, Singh A, Yuanhua L (2020) Inhibitive effect of onion mesocarp extract-nickel nanoparticles composite on simultaneous

- hydrogen production and pipework corrosion in 1 M HCl. *Int J Hydro Energy* 45:10814
22. Ituen E, Ekemini E, Yuanhua L, Singh A (2020) Green synthesis of Citrus reticulata peels extract silver nanoparticles and characterization of structural, biocide and anticorrosion properties. *J Mol Struct* 1207:127819
 23. Kwak JH, Seo JM, Kim NH, Arasu MV, Kim S, Yoon MK, Kim SJ (2017) Variation of quercetin glycoside derivatives in three onion (Allium cepa L.) varieties. *Saudi J Biol Sci* 24:1387
 24. Gennaro L, Leonardi C, Esposito F, Salucci M, Maiani G, Quaglia G, Fogliano V (2002) Flavonoid and carbohydrate contents in Tropea red onions: effects of homelike peeling and storage. *J Agric Food Chem* 50:1904
 25. Khadom AA, Abd AN, Ahmed NA (2018) Xanthium strumarium leaves extracts as a friendly corrosion inhibitor of low carbon steel in hydrochloric acid: Kinetics and mathematical studies. *South African J Chem Eng* 25:13
 26. James AO, Akaranta O (2009) Corrosion inhibition of aluminum in 2.0 M hydrochloric acid solution by the acetone extract of red onion skin. *African J Pure Appl Chem* 3:262
 27. Ong CC, Karim KA (2017) Inhibitory effect of red onion skin extract on the corrosion of mild steel in acidic medium. *Chem Eng Transac* 56:913
 28. Iroha NB, Akaranta O, James AO (2012) Red onion skin extract-furfural resin as corrosion inhibitor for aluminium in acid medium. *Der Chem Sinica* 3:995
 29. Singh A, Ituen EB, Ansari KR, Chauhan DS, Quraishi MA (2019) Surface protection of X80 steel using Epimedium extract and its iodide-modified composites in simulated acid wash solution: a greener approach towards corrosion inhibition. *New J Chem* 43:8527
 30. Huang J, Li Q, Sun D, Lu Y, Su Y, Yang X, Wang H, Wang Y, Shao W, He N, Hong J (2007) Biosynthesis of silver and gold nanoparticles by novel sundried Cinnamomum camphora leaf. *Nanotechnology* 18:105104
 31. Rajakumar G, Rahuman AA (2011) Larvicidal activity of synthesized silver nanoparticles using Eclipta prostrata leaf extract against filariasis and malaria vectors. *Acta Trop* 118:196
 32. Sukirtha R, Priyanka KM, Antony JJ, Kamalakkannan S, Thangam R, Gunasekaran P, Krishnamn M, Achiraman S (2012) Cytotoxic effect of Green synthesized silver nanoparticles using Melia azedarach against in vitro HeLa cell lines and lymphoma mice model. *Proc Biochem* 47:273
 33. Saxena A, Tripathi RM, Zafar F, Singh P (2012) Green synthesis of silver nanoparticles using aqueous solution of Ficus benghalensis leaf extract and characterization of their antibacterial activity. *Mater Let* 67:91
 34. Nabikhan A, Kandasamy K, Raj A, Alikunhi NM (2010) Synthesis of antimicrobial silver nanoparticles by callus and leaf extracts from saltmarsh plant, Sesuvium portulacastrum L. *Colloids Surf B Biointerf* 79:488
 35. Prabu HJ, Johnson I (2015) Plant-mediated biosynthesis and characterization of silver nanoparticles by leaf extracts of Tragia involucrata, Cymbopogon citronella, Solanum verbascifolium and Tylophora ovata. *Karbala Int J Modern Sci* 1:237
 36. Karthiga P (2018) Preparation of silver nanoparticles by Garcinia mangostana stem extract and investigation of the antimicrobial properties. *Biotechnol Res Innov* 2:30
 37. Sur UK, Ankamwar B, Karmakar S, Halder A, Das P (2018) Green synthesis of Silver nanoparticles using the plant extract of Shikakai and Reetha. *Mater Today Proceed* 5:2321
 38. Behravan M, Panahi AH, Naghizadeh A, Ziaee M, Mahdavi R, Mirzapour A (2019) Facile green synthesis of silver nanoparticles using Berberis vulgaris leaf and root aqueous extract and its antibacterial activity. *Int J Biol Macromol* 124:148
 39. Gul S, Ismail M, Khan MI, Khan SB, Asiri AM, Rahman IU, Khan MA, Kamboh MA (2016) Novel synthesis of silver nanoparticles using melon aqueous extract and evaluation of their feeding deterrent activity against housefly Musca domestica. *Asian Pac J Trop Dis* 6:311
 40. Banala RR, Nagati VB, Karnati PR (2015) Green synthesis and characterization of Carica papaya leaf extract coated silver nanoparticles through X-ray diffraction, electron microscopy and evaluation of bactericidal properties. *Saudi J Biol Sci* 22:637
 41. Saber H, Alwaleed EA, Ebnalwaleed KA, Sayed A, Salem W (2017) Efficacy of silver nanoparticles mediated by Jania rubens and Sargassum dentifolium macroalgae; Characterization and biomedical applications. *Egypt J Basic Appl Sci* 4:249
 42. Vijayakumar S (2019) Eco-friendly synthesis of gold nanoparticles using fruit extracts and in vitro anticancer studies. *J Saudi Chem Soc* 23:753
 43. Xu X, Singh A, Sun Z, Ansari KR, Lin Y (2017) Theoretical, thermodynamic and electrochemical analysis of biotin drug as an impending corrosion inhibitor for mild steel in 15% hydrochloric acid. *RSC Open Sci* 4:170933
 44. Nayak D, Ashe S, Rauta PR, Kumari M, Nayak B (2016) Bark extract mediated green synthesis of silver nanoparticles: evaluation of antimicrobial activity and antiproliferative response against osteosarcoma. *Mater Sci Eng C* 58:44
 45. Ituen E, Mkpene V, Ekemini E (2019) Corrosion inhibition of X80 steel in simulated acid wash solution using glutathione and its blends: experimental and theoretical studies. *Colloid Surf A Physicochem Eng Asp* 578:123597
 46. Pontaza-Li' cona YS, Ramos-Jacques AL, Cervantes-Chavez JA, López-Miranda JL, de Jesús R-B Á, Maya-Cornejo J, Hernandez-Martínez AR (2019) Alcoholic extracts from Paulownia tomentosa leaves for silver nanoparticles synthesis. *Res Phys* 12:1670
 47. Ituen E, Mkpene V, Moses E, Obot I (2019) Electrochemical kinetics, molecular dynamics, adsorption and anticorrosion behavior of melatonin biomolecule on steel surface in acidic medium. *Bioelectrochem* 129:42
 48. Umoren SA, Ogbobe O, Okafor PC, Ebenso EE (2017) Polyethylene glycol and polyvinyl alcohol as corrosion inhibitors for aluminium in acidic medium. *J Appl Polym Sci* 105:3363
 49. Dohare P, Quraishi MA, Obot IB (2018) A combined electrochemical and theoretical study of pyridine-based Schiff bases as novel corrosion inhibitors for mild steel in hydrochloric acid medium. *J Chem Sci* 130:8
 50. Ituen E, Mkpene V, Yuanhua L, Singh A (2020) Inhibition of erosion corrosion of pipework steel in descaling solution using 5-hydroxytryptamine-based additives: empirical and computational studies. *J Mol Struct* 1204:127562
 51. Gao H, Xie N, Zhang J, Sun J, Zhang J, Jin Z (2020) Synthesis and application of carboxyethylthiosuccinic acid by thiol-ene click reaction: as a novel rust remover with corrosion inhibition properties. *J Chem Sci* 132:1
 52. Mobin M, Basik M, Shoeb M (2019) A novel organic-inorganic hybrid complex based on Cissus quadrangularis plant extract and zirconium acetate as a green inhibitor for mild steel in 1 M HCl solution. *Appl Surf Sci* 469:38
 53. Ituen EB, James AO, Akaranta O (2017) Fluvoxamine-based corrosion inhibitors for J55 steel in aggressive oil and gas well treatment fluids. *Egypt J Petrol* 26:745
 54. Benardos PG, Vosniakos GC (2003) Predicting surface roughness in machining: a review. *Int J Mach Tools Manufac* 43:833
 55. Sahin Y, Motorcu AR (2005) Surface roughness model for machining mild steel with coated carbide tool. *Mater Design* 26:321
 56. Umoren SA, Solomon MM, Obot IB, Suleiman RK (2019) A critical review on the recent studies on plant biomaterials as corrosion inhibitors for industrial metals. *J Ind Eng Chem* 76:91

57. Liao LL, Mo S, Luo HQ, Li NB (2017) Longan seed and peel as environmentally friendly corrosion inhibitor for mild steel in acid solution: experimental and theoretical studies. *J Colloid Interf Sci* 499:110
58. Ji G, Anjum S, Sundaram S, Prakash R (2015) *Musa paradisica* peel extract as green corrosion inhibitor for mild steel in HCl solution. *Corros Sci* 90:107
59. Prabakaran M, Kim SH, Oh YT, Raj V, Chung IM (2017) Anticorrosion properties of momilactone A isolated from rice hulls. *J Ind Eng Chem* 45:380
60. Odewunmi NA, Umoren SA, Gasem ZM (2015) Watermelon waste products as green corrosion inhibitors for mild steel in HCl solution. *J Environ Chem Eng* 3:286
61. Srivastava M, Tiwari P, Srivastava SK, Kumar A, Ji G, Prakash R (2018) Low cost aqueous extract of *Pisum sativum* peels for inhibition of mild steel corrosion. *J Mol Liq* 254:357
62. Alvarez APE, Fiori-bimbi MV, Neske A, Brand SA, Gervasi CA, Brand SA (2018) *Rollinia occidentalis* extract as green corrosion inhibitor for carbon steel in HCl solution. *J Ind Eng Chem* 58:92
63. Ituen E, Mkpenie V, Ekemini E (2019) Adsorptive Fe-nanoparticles mediated by *Musa sapientum* peels extract as anticorrosion additive for aqueous oilfield descaling solution. *Scientif Afr* 3:e00075

Publisher's Note Springer Nature remains neutral with regard to jurisdictional claims in published maps and institutional affiliations.